





## Article

# Wear Behavior of a Heat-Treatable Al-3.5Cu-1.5Mg-1Si Alloy Manufactured by Selective Laser Melting

Pei Wang <sup>1,2</sup>, Yang Lei <sup>1</sup>, Jun-Fang Qi <sup>1</sup>, Si-Jie Yu <sup>1</sup>, Rossitza Setchi <sup>3</sup>, Ming-Wei Wu <sup>4,\*</sup>, Jürgen Eckert <sup>5,6,\*</sup>, Hai-Chao Li <sup>7</sup> and Sergio Scudino <sup>2</sup>

<sup>1</sup> Additive Manufacturing Institute, College of Mechatronics and Control Engineering, Shenzhen University, Shenzhen 518060, China; peiwang@szu.edu.cn (P.W.); leiyang\_szu@163.com (Y.L.); qijunfangtx@163.com (J.-F.Q.); yusijie1@email.szu.edu.cn (S.-J.Y.)

<sup>2</sup> Institute for Complex Materials, Leibniz IFW Dresden, Helmholtzstraße 20, 01069 Dresden, Germany; s.scudino@ifw-dresden.de

<sup>3</sup> Cardiff School of Engineering, Cardiff University, Cardiff CF24 3AA, UK; Setchi@cardiff.ac.uk

<sup>4</sup> Department of Materials and Mineral Resources Engineering, National Taipei University of Technology, No. 1, Sec. 3, Zhong-Xiao E. Rd., Taipei 10608, Taiwan

<sup>5</sup> Erich Schmid Institute of Materials Science, Austrian Academy of Sciences, Jahnstraße 12, A-8700 Leoben, Austria

<sup>6</sup> Department of Materials Science, Chair of Materials Physics, Montanuniversität Leoben, Jahnstraße 12, A-8700 Leoben, Austria

<sup>7</sup> School of Materials Engineering, Shanghai University of Engineering Science, Shanghai 201620, China; 007lihaichao@163.com

\* Correspondence: mwww@mail.ntut.edu.tw (M.-W.W.); juergen.eckert@unileoben.ac.at (J.E.)

† Adjunct with National University of Science and Technology «MISIS», Leninsky Prosp., 4, 119049 Moscow, Russia.



**Citation:** Wang, P.; Lei, Y.; Qi, J.-F.; Yu, S.-J.; Setchi, R.; Wu, M.-W.; Eckert, J.; Li, H.-C.; Scudino, S. Wear Behavior of a Heat-Treatable Al-3.5Cu-1.5Mg-1Si Alloy Manufactured by Selective Laser Melting. *Materials* **2021**, *14*, 7048. <https://doi.org/10.3390/ma14227048>

Academic Editors: Ori Yehekel and Amir Mostafaei

Received: 27 September 2021

Accepted: 16 November 2021

Published: 20 November 2021

**Publisher's Note:** MDPI stays neutral with regard to jurisdictional claims in published maps and institutional affiliations.



**Copyright:** © 2021 by the authors. Licensee MDPI, Basel, Switzerland. This article is an open access article distributed under the terms and conditions of the Creative Commons Attribution (CC BY) license (<https://creativecommons.org/licenses/by/4.0/>).

**Abstract:** In this study, the wear behavior of a heat-treatable Al-7Si-0.5Mg-0.5Cu alloy fabricated by selective laser melting was investigated systematically. Compared with the commercial homogenized AA2024 alloy, the fine secondary phase of the SLM Al-Cu-Mg-Si alloy leads to a low specific wear rate ( $1.8 \pm 0.11 \times 10^{-4} \text{ mm}^3(\text{Nm})^{-1}$ ) and a low average coefficient of friction ( $0.40 \pm 0.01$ ). After the T6 heat treatment, the SLM Al-Cu-Mg-Si alloy exhibits a lower specific wear rate ( $1.48 \pm 0.02 \times 10^{-4} \text{ mm}^3(\text{Nm})^{-1}$ ), but a similar average coefficient of friction ( $0.34 \pm 0.01$ ) as the heat-treated AA2024 alloy. Altogether, the SLM Al-3.5Cu-1.5Mg-1Si alloy is suitable for the achievement of not only superior mechanical performance, but also improved tribological properties.

**Keywords:** selective laser melting; Al-Si-Cu-Mg alloy; heat treatment; microstructure; wear behavior

## 1. Introduction

Selective laser melting (SLM) is one of the advanced additive manufacturing technologies that works with the assistance of computer-aided designs (CAD) and has been widely used for the fabrication of metallic components [1,2]. In recent years, the development of novel alloys fabricated by SLM has attracted a lot of attention due to the outstanding advantages of process flexibility, cost reduction, and energy-saving [3,4]. In addition, Al-based alloys have become one of the most researched SLM materials [5,6], due to the demand and widespread applications in the aerospace and automotive industries.

The low density, good castability, and weldability of SLM-processed Al-Si alloys, as well as their high wear and corrosion resistance, have been studied extensively [7,8]. Prashanth et al. [9] revealed that SLM processing of Al-12Si results in a fine cellular structure (cell size of  $1 \pm 0.3 \mu\text{m}$ ) yielding three-times higher strength values than the yield strength (260 MPa) of conventional cast samples. Moreover, the tribological properties of Al-12Si samples produced by SLM were evaluated via sliding and fretting wear tests and weight loss experiments, revealing that the as-prepared SLM samples show better wear resistance than their cast counterparts [10]. Similar to SLM Al-12Si, SLM Al-10Si-Mg can also achieve

a higher strength reaching up to 500 MPa and a significantly improved wear resistance due to the finer microstructure of the SLM material [11–13]. In fact, almost all Al-Si and Al-Si-Mg series alloys, such as Al-35Si, Al-50Si, and Al-7Si-Mg, have significantly higher mechanical performance and wear resistance compared with the Al-Cu and Al-Zn series alloys [14–16]. However, the mechanical properties and wear resistance of the current Al-Si and Al-Si-Mg series alloys need additional effort to be tailored to meet the demands that the Al-based alloys require under working conditions [11,17,18].

In recent years, Al-Cu series aluminum alloys have been researched due to their good heat treatability, excellent specific strength, and good damage tolerance [19–21]. However, the elimination of cracks in Al-Cu series aluminum alloys resulting from the high cooling rate of SLM ( $10^4$ – $10^5$  K/s [22]) is considered as the most important challenge of Al-Cu series aluminum alloys that are fabricated by SLM. Furthermore, Al-Cu series aluminum alloys as construction materials will inevitably encounter friction and wear conditions [1,23]. Therefore, the design and fabrication of SLM Al-Cu series aluminum alloys with high strength and improved wear resistance has important practical significance.

The addition of Si can decrease the melting temperature of Al alloys, which is helpful in decreasing the thermal stresses during the processing of SLM and in refining their grain size. This can prevent hot cracking in SLM Al-Cu alloys during the processing of SLM [17,24]. Moreover, the addition of Si can lead to the formation of  $Mg_2Si$  phase with high melting temperature, low density, high hardness, low thermal expansion coefficient, and reasonably high elastic modulus [25]. The formation of  $Mg_2Si$  phase and the grain refinement of Al alloys may not only contribute to an optimized combination of strength and ductility of Al alloys, but may also improve their wear resistance [26,27]. Therefore, a SLM Al-3.5Cu-1.5Mg-1Si alloy with improved mechanical properties and corrosion resistance was designed and fabricated in our previous work [28,29].

In the present work, the wear resistance of the Al-3.5Cu-1.5Mg-1Si alloy in both as-prepared SLM and heat-treated conditions is investigated systematically and compared with a commercial AA2024 alloy. The effect of microstructural particularities on the wear mechanism of the SLM Al-3.5Cu-1.5Mg-1Si alloy is discussed comprehensively.

## 2. Experimental Details

### 2.1. Materials and SLM Processing

The Al-3.5Cu-1.5Mg-1Si alloy was fabricated using a SLM 250<sup>HL</sup> device (SLM Solutions Group AG, Luebeck, Germany) equipped with a 400 W Nd:YAG laser (continuous wave, IPG Photonics, Massachusetts, USA), using gas-atomized powders (powder size: 20–60  $\mu\text{m}$ ;  $d_{50}$  of the powders:  $41 \pm 1 \mu\text{m}$ ) with a nominal composition of Al-3.5Cu-1.5Mg-1Si (wt%). Figure 1 depicts on the characteristics of the starting gas-atomized Al-3.5Cu-1.5Mg-1Si powder used for SLM processing. More details on the SLM processing of this alloy can be found in [29]. SLM processing was done under protective argon atmosphere with a purity of 99.999%. The oxygen content in the SLM chamber was below 0.02 vol% during the complete processing time.

As reference material, a homogenized commercial AA2024-O alloy was supplied by Harbin Institute of Technology. Details on its exact composition (4.06 wt% Cu, 1.36 wt% Mg, 0.18 wt% Si, and 0.57 wt% Mn) can be found in [28]. In order to improve the mechanical properties, the as-SLM alloy and AA2024-O alloy samples were solution-treated at 793 K for 1 h, water quenched, and then subjected to aging at 463 K for 10 h, followed by air cooling. These heat-treated samples are termed T6.

### 2.2. Characterization

The analysis of phases and structures was performed by X-ray diffraction (XRD; D3290 PANalytical X'pert PRO, Co-K $\alpha$  radiation ( $\lambda = 0.178897 \text{ \AA}$ ), PANalytical, PANalytical, Almelo, The Netherlands) in reflection mode. In order to maintain a uniform sample height, the bulk samples were grinded to  $0.8 \pm 0.1 \text{ mm}$ . The microstructures were characterized by a high-resolution scanning electron microscope (SEM; Gemini LEO 1530 microscope, Carl

Zeiss AG, Oberkochen, Germany). The SEM was equipped with an energy-dispersive X-ray spectroscopy system (EDS; Quantax400 with SDD-Detector Xflash4010, Bruker QUANTAX, Ettlingen, Germany) for element analysis. Based on the imaging principles of SEM, both back-scattered electron (BSE) and secondary electron (SE) modes were used to observe the microstructure.

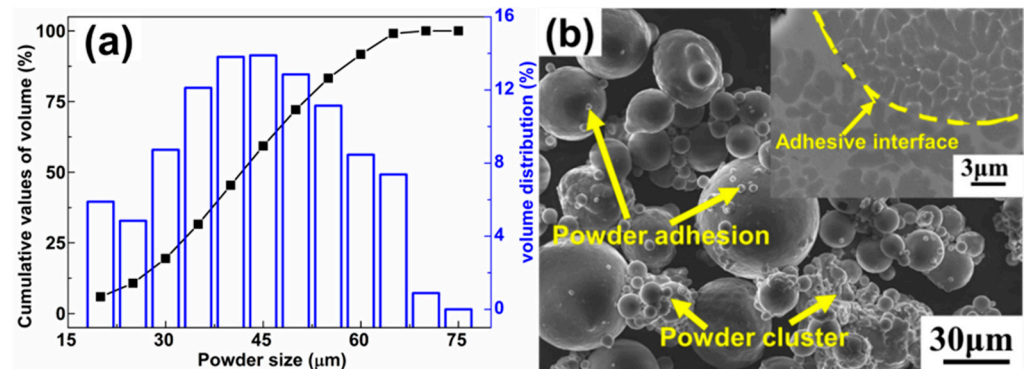


**Figure 1.** (a) Distribution of the powder size; (b) typical morphologies of the starting Al-3.5Cu-1.5Mg-1Si powders (inset: Cross-section of a powder particle).

### 2.3. Mechanical Properties

Vickers microhardness tests were performed using an HMV Shimadzu microhardness tester (Shimadzu Corporation, Tokyo, Japan) with 50 g of load and 10 s of dwell time. The hardness of each sample is the value averaged over at least 20 different points, which were selected automatically. Room-temperature compression tests were carried out with the loading axis parallel to the building direction (BD), using an Instron 5869 machine (Instron, Boston, MA, USA) at a constant crosshead speed of 0.001 mm/s according to the DIN 50106 standard. A laser extensometer (Fiedler Optoelektronik GmbH, Luetzen, Germany) was used to measure the strain directly on the samples. At least five samples were tested in the same condition to ensure the reproducibility of the results.

### 2.4. Sliding Wear Tests

Sliding wear tests were carried out by a pin-on-disk setup with a Tribometer T500 (Nanovea, Irvine, CA, USA) at room temperature, according to DIN EN 1071-13 [30,31]. The temperature was detected to control the temperature during the measurement, which was stabilized in the range of 313–323 K. Pin samples made from the tested alloys ( $\text{Ø}6 \times 30$  mm) and a X210Cr12 steel grinding disk (hardness of 57–62 HRC and elasticity modulus of 210–218 GPa) were used for the measurements, which were performed with the setup shown in Figure 2. Before the wear tests, the samples were grinded by the SiC grinding paper with a final finish of 1200 grit (P4000).

According to DIN EN 1071–13, the specific wear rate  $k$  was calculated as follows:

$$k = \frac{V}{F_N L} \quad (1)$$

A normal load  $F_N$  of 15 N was applied on the lever arm during the measurement. The sliding distance is given by  $L = 2\pi rvt$ , where  $r$  is the radius of the wear track (30 mm),  $v$  is the rotating speed of the disk (400 RPM), and  $t$  is the sliding time (60 min). According to the calculation, the sliding distance ( $L$ ) is 4521 m. Therefore, the wear volume  $V$  was determined for every tested sample by  $V = (m_0 - m)/\rho$ , whereas  $m_0$  and  $\rho$  are the mass of the pin samples before the wear test and their density, and  $m$  is the mass after testing.

In addition, the average value of the coefficient of friction (COF) was measured using a separate load system in contact with the continuous lever arm and recorded by a Nanovea Tribometer system. All of the data (specific wear rate and average COF) shown are averages of at least three different measurements.

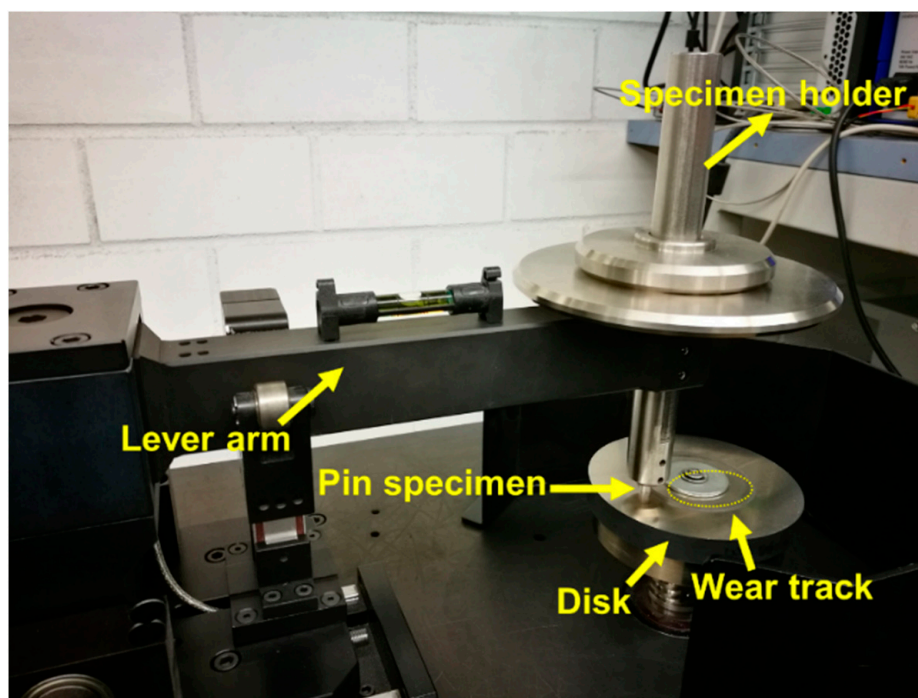


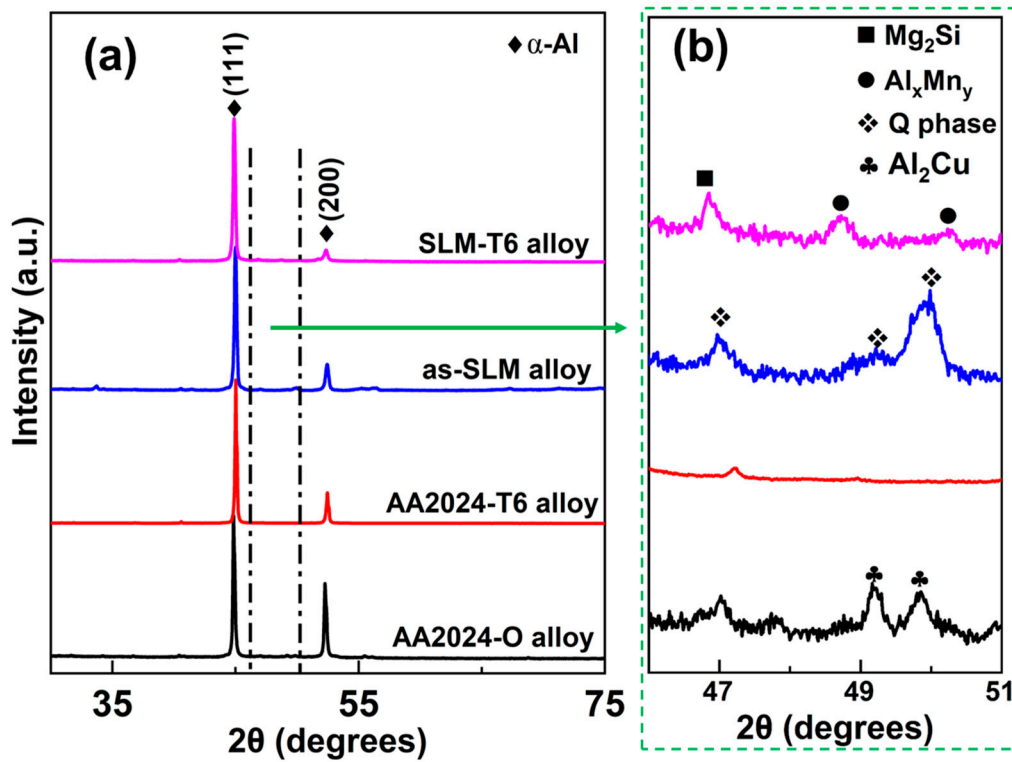
**Figure 2.** Photograph of the pin-on-disk wear test setup.

### 3. Results and Discussion

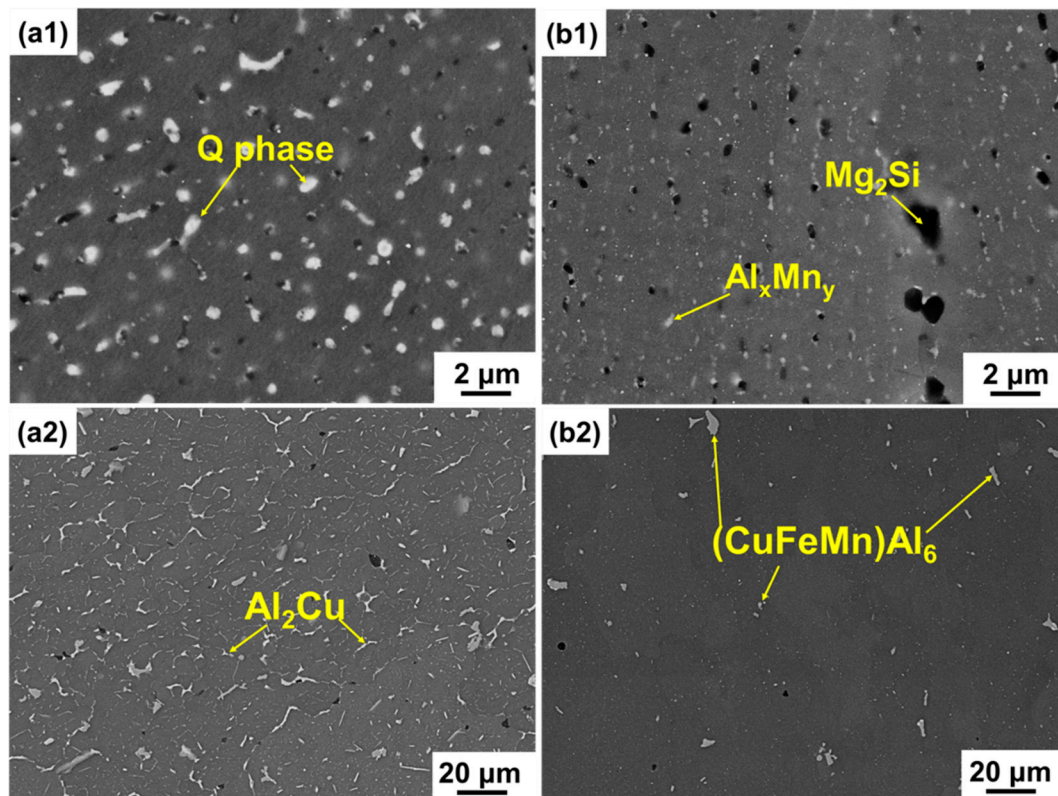
The phase analysis of all the materials is shown in Figure 3, which contains the  $\alpha$ -Al phase and Q phase in the XRD patterns of the as-SLM samples [29,32]. After the T6 heat treatment, the SLM-T6 alloy shows the following phases:  $\alpha$ -Al,  $Mg_2Si$  (Fm-3m [32,33]), and  $Al_xMn_y$  (unknown space group), suggesting that the Q phase transforms to  $Mg_2Si$  and  $Al_xMn_y$ . The details of the phase transformation were discussed in [29]. As shown in Figure 3, there are  $\alpha$ -Al and  $Al_2Cu$  phases in the AA2024-O alloy and the  $Al_2Cu$  phases disappear after the T6 treatment. Moreover, the phase with the peak at  $47^\circ$  cannot be identified unambiguously by the X'pert high scores (version 5.1.0, PANalytical, Almelo, The Netherlands) software. Furthermore, from References [34–36], there is only very limited information on this phase. Therefore, the phases with the peak at  $47^\circ$  in AA2024-O and AA2024-T6 were neglected in the XRD patterns.

Figure 4 shows the typical microstructures of the SLM Al-Cu-Mg-Si alloy and the AA2024-O alloy before and after the T6 heat treatment. The nano-sized Q phase (around 300 nm), which contains Al, Cu, Mg, and Si elements, is generated in the Al matrix of the as-SLM alloy, due to the rapid solidification during the processing of SLM [29,37]. After the T6 heat treatment, the Al matrix shows the formation of the  $Al_2Cu(Mg)$  ( $\theta'$  and  $S'$ ) phase in the SLM-T6 alloy, which leads to a significant improvement of the tensile strength [29]. In addition, the heat treatment results in transformation of the fine Q phase into  $Mg_2Si$  and  $Al_xMn_y$  (Figure 4b1). It should be mentioned that the formation of these phases, especially of the  $Mg_2Si$  phase, has a significant importance in improving the friction and wear properties of Al-Cu-Mg-Si alloys [38]. Compared with the as-SLM alloy, the white  $\theta$ - $Al_2Cu$  phase (EDS measurement:  $74.7 \pm 1.2$  at% Al and  $24 \pm 1.1$  at% Cu) is the main phase dispersed in the AA2024-O alloy (Figure 4a2). After the T6 heat treatment, the  $Al_2Cu$  phase is dissolved in the Al matrix, and undefined (CuFeMn)Al<sub>6</sub> phases (EDS measurement containing mainly additional  $65.5 \pm 0.4$  at% Al,  $6.2 \pm 0.5$  at% Cu,  $7.4 \pm 0.4$  at% Mn, and  $12.9 \pm 0.4$  at% Fe) are generated. Similar microstructures and phases were described in previous works on the AA2024 alloy [34–36,39,40].





**Figure 3.** XRD patterns of the SLM Al-3.5Cu-1.5Mg-1Si alloy and of the commercial AA2024-O alloy with and without the T6 heat treatment: (a) Overview; and (b) close-up view of the diffraction patterns between  $46^{\circ} \leq 2\theta \leq 51^{\circ}$ .



**Figure 4.** Typical morphologies of the alloys in BSE mode: (a1) The as-SLM alloy; (b1) SLM-T6 alloy; (a2) AA2024-O alloy; (b2) AA2024-T6 alloy.

The microhardness, the average coefficient of friction (average COF), and the specific wear rate of all the alloys are shown in Figure 5. The microhardness, the average COF, and the specific wear rate of the AA2024-O alloy and the AA2024-T6 alloy are  $73 \pm 1 \text{ HV}_{0.05}$ ,  $0.47 \pm 0.02$ ,  $2.23 \pm 0.01 \times 10^{-4} \text{ mm}^3(\text{Nm})^{-1}$  and  $179 \pm 1 \text{ HV}_{0.05}$ ,  $0.36 \pm 0.01$ ,  $1.74 \pm 0.08 \times 10^{-4} \text{ mm}^3(\text{Nm})^{-1}$ , respectively. Evidently, the as-SLM alloy has a higher hardness ( $124 \pm 1 \text{ HV}_{0.05}$ ), lower average COF ( $0.40 \pm 0.01$ ), and lower specific wear rate ( $1.8 \pm 0.11 \times 10^{-4} \text{ mm}^3(\text{Nm})^{-1}$ ) than the AA2024-O alloy. After the T6 heat treatment, with the increasing hardness of the SLM-T6 alloy to ( $176 \pm 1 \text{ HV}_{0.05}$ ), the average COF and the specific wear rate decrease to  $0.34 \pm 0.01$  and  $1.48 \pm 0.02 \times 10^{-4} \text{ mm}^3(\text{Nm})^{-1}$ , respectively. The formation of nano- $\text{Al}_2\text{Cu}$  (Mg) precipitates in the AA2024-T6 alloy and the SLM-T6 alloy enhances the mechanical properties. According to the classical Archard's equation, the coefficient of friction and the wear loss of a material is inversely proportional to its hardness under adhesive wear conditions [41–43]. Therefore, after the heat treatment, the strengthened Al matrix of the SLM-T6 alloy results in an improvement of its frictional and wear properties. It is striking that the AA2024-T6 alloy has a slightly higher hardness, but a relatively lower specific wear rate than the SLM-T6 alloy. In general, the higher Cu and Mg contents (Cu:  $4.06 \pm 0.01 \text{ wt\%}$ , Mg:  $1.36 \pm 0.01 \text{ wt\%}$  [28]) in the AA2024-T6 alloy can result in more nano- $\text{Al}_2\text{Cu}$  (Mg) precipitates in the Al-matrix than the SLM-T6 alloy, contributing to the higher hardness of the AA2024-T6 alloy [44,45]. However, due to the positive effect of the solid solution of Si on the wear properties of the Al-Cu-Mg alloy [38,46,47], the high Si content in the SLM-T6 alloy, especially the formation of  $\text{Mg}_2\text{Si}$  (Figure 4a2), can lead to a lower average COF and specific wear rate than the AA2024-T6 alloy.

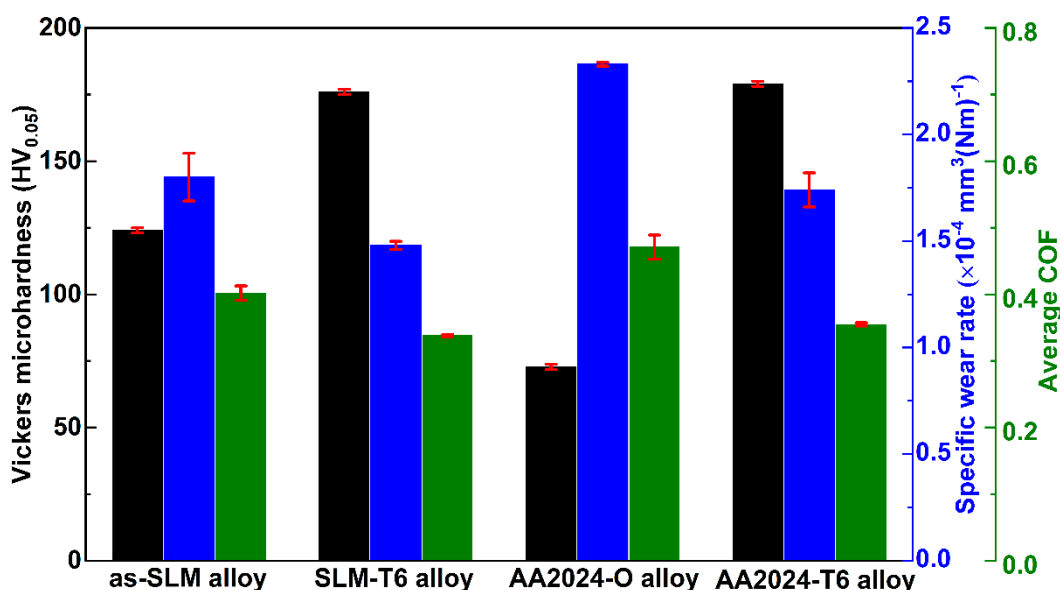
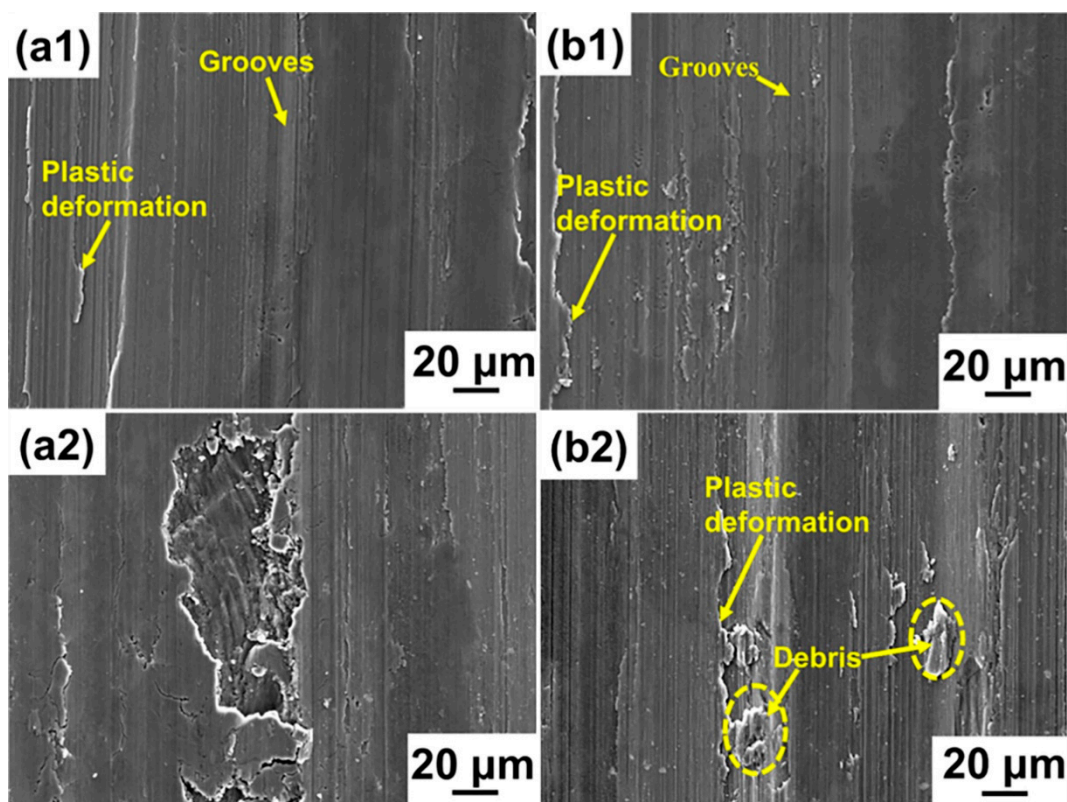


Figure 5. Microhardness, average coefficient of friction (average COF), and specific wear rate of all the samples.

In addition, after the heat treatment, the Q phase in the as-SLM alloy dissolves into the Al matrix, and is accompanied by the disappearance of the classical layer-by-layer microstructure generated during the processing of SLM. Moreover, the nano-precipitates are dispersed uniformly to strengthen the Al matrix [29]. The disappearance of the layer-by-layer microstructure results in a lower standard error of the average of the COF SLM-T6 alloy and a specific wear rate than the as-SLM alloy.

In order to compare the wear mechanism of the SLM materials with the commercial alloy, the worn surfaces of all the materials are shown in Figure 6. The grooves in the as-SLM alloy are slim, resulting in a smooth worn surface. After the T6 heat treatment, the wear debris is very fine and the surface is smoother than the as-SLM alloy without the heat treatment. Despite the existence of fine debris for the SLM-T6 alloy, the morphologies of the SLM Al-Cu-Mg-Si specimens with and without the heat treatment mainly show

typical abrasive wear features. For comparison, the surface of the AA2024-O alloy not only shows large grooves resulting from plastic deformation, but also a sizeable amount of large debris, representing a classical mixed worn morphology, indicative of abrasive and adhesive mechanisms. Although the formation of the nano-precipitates after the T6 heat treatment improves the hardness of the Al matrix, there is still a sizeable amount of large debris and only an insignificant plastic deformation for the AA2024-T6 alloy. This indicates that despite the improved mechanical properties of the AA2024-T6 alloy, the main wear mechanism of this alloy does not change. The morphological comparison of the SLM-T6 and AA2024-T6 alloys provides evidence for the poor wear properties of the AA2024-T6 alloy despite its higher hardness.



**Figure 6.** SEM morphologies of the worn surfaces in SE mode: (a1) The as-SLM alloy; (b1) SLM-T6 alloy; (a2) AA2024-O alloy; (b2) AA2024-T6 alloy.

In order to analyze the influence of the different phases on the features observed on the worn surfaces and the wear properties, the worn surfaces of the samples at high magnification are shown in Figure 7. The fine Q phase ( $\sim 200$  nm) is embedded into the grooves of the Al matrix after the wear test. After the T6 heat treatment, the grooves only exhibit the area around the  $Mg_2Si$  phase. As shown in (Figure 7b1), the observation of the grooves is difficult around these fine phases, due to the smaller size of the  $Al_xMn_y$  phase. The morphologies at high magnification indicate that the small size of the Q and  $Mg_2Si$  phases, respectively, lead to slim grooves and smooth worn surfaces for the as-SLM and the SLM-T6 alloys. Compared with the as-SLM alloy, the large  $Al_2Cu$  phase ( $\geq 2$   $\mu m$ ) in the AA2024-O alloy is fragmented during the wear test and the pieces of the  $Al_2Cu$  phase are embedded into the Al matrix. Therefore, due to the synergistic effect of the crushed  $Al_2Cu$  hard phase and the soft Al matrix, the large debris is cut off from the matrix, and subsequently attached on the Al matrix during the wear test (Figure 7a2). Despite the effect of the heat treatment on the strengthening of the Al matrix, the adhesive phenomenon is reduced, but still a few large debris on the worn surface are visible due to the large size of the  $(CuFeMn)Al_6$  phase (Figure 7b2). According to the above analyses, compared with the



commercial AA2024 alloy at the same heat treatment condition, the fine phases can result in the improvement of the wear resistance of the SLM Al-Cu-Mg-Si alloy.

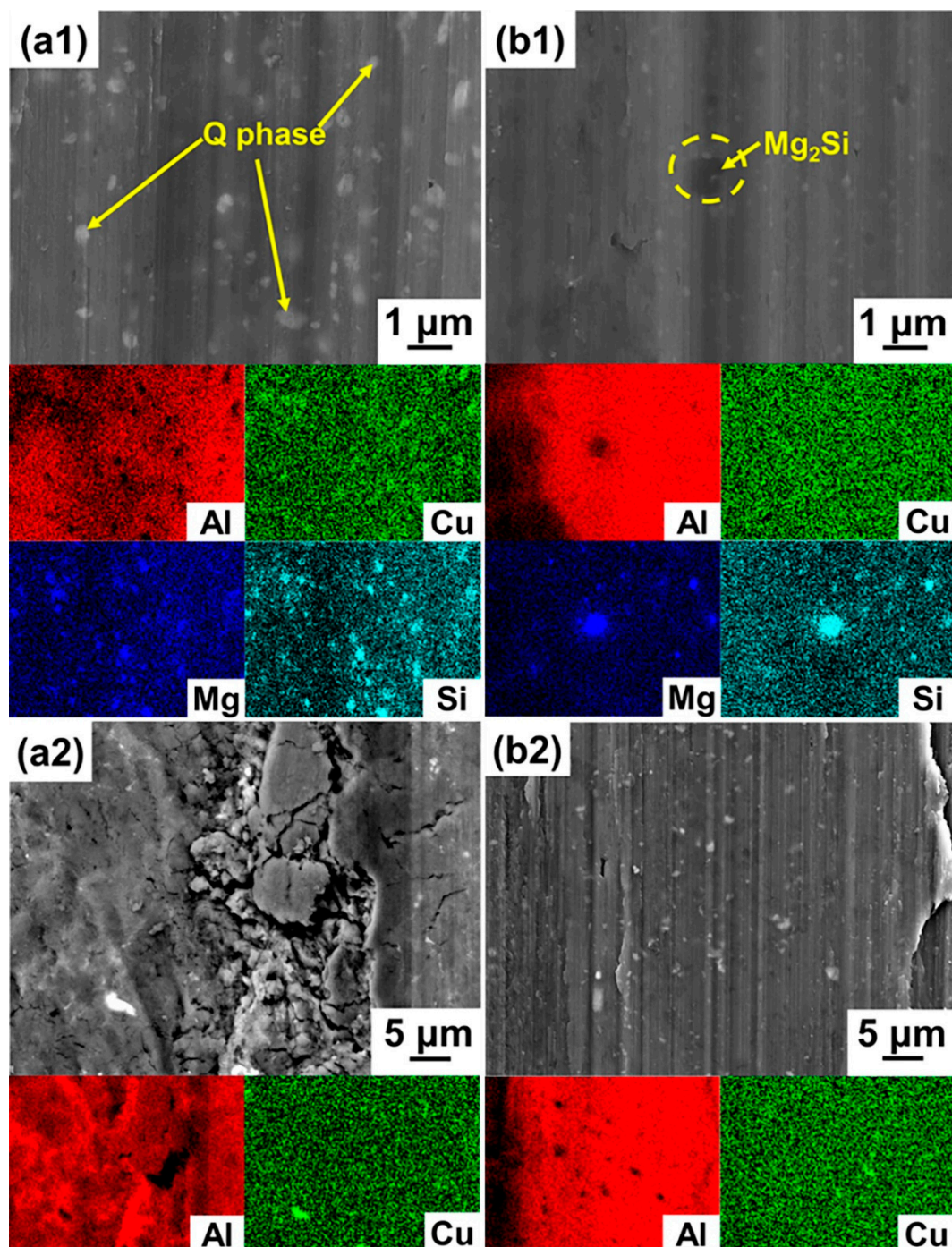


**Figure 7.** SEM close-up view and EDS maps at high magnification in SE mode: (a1) The as-SLM alloy; (b1) SLM-T6 alloy; (a2) AA2024-O alloy; (b2) AA2024-T6 alloy.

#### 4. Conclusions

In this study, the wear resistance of the SLM Al-3.5Cu-1.5Mg-1Si alloy with and without the T6 heat treatment was investigated and their wear mechanisms were discussed. The nano-size Q phase generated during the processing of SLM causes the SLM Al-Cu-Mg-Si alloy to have a better specific wear rate ( $1.8 \pm 0.11 \times 10^{-4} \text{ mm}^3(\text{Nm})^{-1}$ ) and average of coefficient of friction ( $0.40 \pm 0.01$ ) than the conventional AA2024-O alloy at the same



heat treatment condition. After the T6 heat treatment, nano-sized  $\text{Al}_2\text{Cu}(\text{Mg})$  and nano-sized  $\text{Mg}_2\text{Si}$  phases precipitate in the matrix, which lead to the improvement of the wear resistance, i.e., the average COF and the specific wear rate decrease to  $0.34 \pm 0.01$  and  $1.48 \pm 0.02 \times 10^{-4} \text{ mm}^3(\text{Nm})^{-1}$ . The morphologies after the wear tests of the SLM Al-3.5Cu-1.5Mg-1Si alloys with and without the T6 heat treatment both show a typical plastic deformation with slim grooves, indicating the occurrence of an abrasive mechanism.

**Author Contributions:** Conceptualization, P.W. and S.S.; methodology, J.E. and S.S.; formal analysis, S.-J.Y. and H.-C.L.; investigation, Y.L. and J.-F.Q.; data curation, Y.L., S.-J.Y. and J.-F.Q.; writing—original draft preparation, P.W. and J.E.; writing—review and editing, J.E. and R.S.; project administration, P.W., J.E. and M.-W.W.; funding acquisition, P.W., J.E. and M.-W.W. All authors have read and agreed to the published version of the manuscript.

**Funding:** This work was supported by the National Natural Science Foundation of China (NSFC, No. 52105385 and No. 51971149), the Guangdong Basic and Applied Basic Research Foundation (2020A1515110869), Shenzhen International Cooperation Research (GJHZ20190822095418365), and the Natural Science Foundation of SZU (Grant No. 2019040). Additional support was provided by the European Regional Development Fund (ASTRA6-6), and the ASTUTE programme on Advanced and Sustainable Manufacturing Technologies funded by the European Union through the Welsh European Funding Office and Science and Technology Innovation Commission of Shenzhen (No. KQJSCX20180328095612712). J. Eckert is grateful for the support from the Ministry of Science and Higher Education of the Russian Federation in the framework of the Increase Competitiveness Program of MISiS (Support project for young research engineers, project no. K2-2020-046). This work was also supported by the National Taipei University of Technology-Shenzhen University Joint Research Program (project number NTUT-SZU-108-11).

**Institutional Review Board Statement:** Not applicable.

**Informed Consent Statement:** Not applicable.

**Data Availability Statement:** The raw data required to reproduce these results cannot be shared at this time as the data also forms part of an ongoing study.

**Conflicts of Interest:** The authors declare no conflict of interest.

## References

1. Wang, P.; Eckert, J.; Prashanth, K.G.; Wu, M.W.; Kaban, I.; Xi, L.X.; Scudino, S. A review of particulate-reinforced aluminum matrix composites fabricated by selective laser melting. *Trans. Nonferrous Met. Soc.* **2020**, *30*, 2001–2034. [[CrossRef](#)]
2. Yu, W.H.; Sing, S.L.; Chua, C.K.; Kuo, C.N.; Tian, X.L. Particle-reinforced metal matrix nanocomposites fabricated by selective laser melting: A state of the art review. *Prog. Mater. Sci.* **2019**, *104*, 330–379. [[CrossRef](#)]
3. Wang, P.; Lao, C.S.; Chen, Z.W.; Liu, Y.K.; Wang, H.; Wendrock, H.; Eckert, J.; Scudino, S. Microstructure and mechanical properties of Al-12Si and Al-3.5Cu-1.5Mg-1Si bimetal fabricated by selective laser melting. *J. Mater. Sci. Technol.* **2020**, *36*, 18–26. [[CrossRef](#)]
4. Wang, P.; Chen, F.H.; Eckert, J.; Pilz, S.; Scudino, S.; Prashanth, K.G. Microstructural evolution and mechanical properties of selective laser melted Ti-6Al-4V induced by annealing treatment. *J. Cent. South Univ.* **2021**, *28*, 1068–1077. [[CrossRef](#)]
5. Bartkowiak, K.; Ullrich, S.; Frick, T.; Schmidt, M. New Developments of Laser Processing Aluminium Alloys via Additive Manufacturing Technique. *Phys. Procedia* **2011**, *12*, 393–401. [[CrossRef](#)]
6. Kruth, J.P.; Levy, G.; Klocke, F.; Childs, T.H.C. Consolidation phenomena in laser and powder-bed based layered manufacturing. *CIRP Ann. Manuf. Technol.* **2007**, *56*, 730–759. [[CrossRef](#)]
7. Thijs, L.; Kempen, K.; Kruth, J.P.; van Humbeeck, J. Fine-structured aluminium products with controllable texture by selective laser melting of pre-alloyed AlSi10Mg powder. *Acta Mater.* **2013**, *61*, 1809–1819. [[CrossRef](#)]
8. Zhang, J.L.; Song, B.; Wei, Q.S.; Bourell, D.; Shi, Y.S. A review of selective laser melting of aluminum alloys: Processing, microstructure, property and developing trends. *J. Mater. Sci. Technol.* **2019**, *35*, 270–284. [[CrossRef](#)]
9. Prashanth, K.G.; Scudino, S.; Klauss, H.J.; Surreddi, K.B.; Löber, L.; Wang, Z.; Chaubey, A.K.; Kühn, U.; Eckert, J. Microstructure and mechanical properties of Al-12Si produced by selective laser melting: Effect of heat treatment. *Mater. Sci. Eng. A* **2014**, *590*, 153–160. [[CrossRef](#)]
10. Prashanth, K.G.; Debalina, B.; Wang, Z.; Gostin, P.F.; Gebert, A.; Calin, M.; Kühn, U.; Kamaraj, M.; Scudino, S.; Eckert, J. Tribological and corrosion properties of Al-12Si produced by selective laser melting. *J. Mater. Res.* **2014**, *29*, 2044–2054. [[CrossRef](#)]
11. Li, W.; Li, S.; Liu, J.; Zhang, A.; Zhou, Y.; Wei, Q.S.; Yan, C.Z.; Shi, Y.S. Effect of heat treatment on AlSi10Mg alloy fabricated by selective laser melting: Microstructure evolution, mechanical properties and fracture mechanism. *Mater. Sci. Eng. A* **2016**, *663*, 116–125. [[CrossRef](#)]

12. Chen, B.; Moon, S.K.; Yao, X.; Bi, G.; Shen, J.; Umeda, J.; Kondoh, K. Strength and strain hardening of a selective laser melted AlSi10Mg alloy. *Scr. Mater.* **2017**, *141*, 45–49. [[CrossRef](#)]
13. Dai, D.H.; Gu, D.D.; Zhang, H.; Xiong, J.P.; Ma, C.L.; Hong, C.; Poprawe, R. Influence of scan strategy and molten pool configuration on microstructures and tensile properties of selective laser melting additive manufactured aluminum based parts. *Opt. Lasers Eng.* **2018**, *99*, 91–100. [[CrossRef](#)]
14. Jia, Y.D.; Ma, P.; Prashanth, K.G.; Wang, G.; Yi, J.; Scudino, S.; Cao, F.Y.; Sun, J.F.; Eckert, J. Microstructure and thermal expansion behavior of Al-50Si synthesized by selective laser melting. *J. Alloys Compd.* **2017**, *699*, 548–553. [[CrossRef](#)]
15. Yang, K.V.; Rometsch, P.; Jarvis, T.; Rao, J.; Cao, S.; Davies, C.; Wu, X.H. Porosity formation mechanisms and fatigue response in Al-Si-Mg alloys made by selective laser melting. *Mater. Sci. Eng. A* **2018**, *712*, 166–174. [[CrossRef](#)]
16. Rao, H.; Giet, S.; Yang, K.; Wu, X.H.; Davies, C.H.J. The influence of processing parameters on aluminium alloy A357 manufactured by Selective Laser Melting. *Mater. Des.* **2016**, *109*, 334–346. [[CrossRef](#)]
17. Kimura, T.; Nakamoto, T.; Mizuno, M.; Araki, H. Effect of silicon content on densification, mechanical and thermal properties of Al-xSi binary alloys fabricated using selective laser melting. *Mater. Sci. Eng. A* **2017**, *682*, 593–602. [[CrossRef](#)]
18. Rao, J.H.; Zhang, Y.; Zhang, K.; Huang, A.J.; Davies, C.H.J.; Wu, X.H. Multiple precipitation pathways in an Al-7Si-0.6Mg alloy fabricated by selective laser melting. *Scr. Mater.* **2019**, *160*, 66–69. [[CrossRef](#)]
19. Tan, Q.Y.; Zhang, J.Q.; Sun, Q.; Fan, Z.Q.; Li, G.; Yin, Y.; Liu, Y.A.; Zhang, M.X. Inoculation treatment of an additively manufactured 2024 aluminium alloy with titanium nanoparticles. *Acta Mater.* **2020**, *196*, 1–16. [[CrossRef](#)]
20. Gharbi, O.; Jiang, D.; Feenstra, D.R.; Kairy, S.K.; Wu, Y.; Hutchinson, C.R.; Birbilis, N. On the corrosion of additively manufactured aluminium alloy AA2024 prepared by selective laser melting. *Corros. Sci.* **2018**, *143*, 93–106. [[CrossRef](#)]
21. Wang, P.; Deng, L.; Prashanth, K.G.; Pauly, S.; Eckert, J.; Scudino, S. Microstructure and mechanical properties of Al-Cu alloys fabricated by selective laser melting of powder mixtures. *J. Alloys Compd.* **2018**, *735*, 2263–2266. [[CrossRef](#)]
22. Pauly, S.; Wang, P.; Kühn, U.; Kosiba, K. Experimental determination of cooling rates in selectively laser-melted eutectic Al-33Cu. *Addit. Manuf.* **2018**, *22*, 753–757. [[CrossRef](#)]
23. Fiocchi, J.; Tuissi, A.; Biffi, C.A. Heat treatment of aluminium alloys produced by laser powder bed fusion: A review. *Mater. Des.* **2021**, *204*, 109651. [[CrossRef](#)]
24. Zhou, S.Y.; Su, Y.; Wang, H.; Enz, J.; Ebel, T.; Yan, M. Selective laser melting additive manufacturing of 7xxx series Al-Zn-Mg-Cu alloy: Cracking elimination by co-incorporation of Si and TiB<sub>2</sub>. *Addit. Manuf.* **2020**, *36*, 101458. [[CrossRef](#)]
25. Qin, Q.D.; Zhao, Y.G.; Zhou, W. Dry sliding wear behavior of Mg<sub>2</sub>Si/Al composites against automobile friction material. *Wear* **2008**, *264*, 654–661. [[CrossRef](#)]
26. Kang, N.; Coddet, P.; Chen, C.Y.; Wang, Y.; Liao, H.L.; Coddet, C. Microstructure and wear behavior of in-situ hypereutectic Al-high Si alloys produced by selective laser melting. *Mater. Des.* **2016**, *99*, 120–126. [[CrossRef](#)]
27. Li, J.; Cheng, X.; Li, Z.; Zong, X.; Zhang, S.Q.; Wang, H.M. Improving the mechanical properties of Al-5Si-1Cu-Mg aluminum alloy produced by laser additive manufacturing with post-process heat treatments. *Mater. Sci. Eng. A* **2018**, *735*, 408–417. [[CrossRef](#)]
28. Wang, P.; Gebert, A.; Yan, L.; Li, H.C.; Lao, C.S.; Chen, Z.W.; Kosiba, K.; Kühn, U.; Scudino, S. Corrosion of Al-3.5Cu-1.5Mg-1Si alloy prepared by selective laser melting and heat treatment. *Intermetallics* **2020**, *124*, 106871. [[CrossRef](#)]
29. Wang, P.; Gammer, C.; Brenne, F.; Prashanth, K.G.; Mendes, R.G.; Rummeli, M.H.; Gemming, T.; Eckert, J.; Scudino, S. Microstructure and mechanical properties of a heat-treatable Al-3.5Cu-1.5Mg-1Si alloy produced by selective laser melting. *Mater. Sci. Eng. A* **2018**, *711*, 562–570. [[CrossRef](#)]
30. Zeisig, J.; Schädlich, N.; Giebler, L.; Sander, J.; Eckert, J.; Kühn, U.; Hufenbach, J. Microstructure and abrasive wear behavior of a novel FeCrMoVC laser cladding alloy for high-performance tool steels. *Wear* **2017**, *382–383*, 107–112. [[CrossRef](#)]
31. Deng, L.; Gebert, A.; Zhang, L.; Chen, H.Y.; Gu, D.D.; Kühn, U.; Zimmermann, M.; Kosiba, K.; Pauly, S. Mechanical performance and corrosion behaviour of Zr-based bulk metallic glass produced by selective laser melting. *Mater. Des.* **2020**, *189*, 108532. [[CrossRef](#)]
32. Ravi, C.; Wolverton, C. First-principles study of crystal structure and stability of Al-Mg-Si-(Cu) precipitates. *Acta Mater.* **2004**, *52*, 4213–4227. [[CrossRef](#)]
33. Chakrabarti, D.J.; Laughlin, D.E. Phase relations and precipitation in Al-Mg-Si alloys with Cu additions. *Prog. Mater. Sci.* **2004**, *49*, 389–410. [[CrossRef](#)]
34. Goodarzy, M.H.; Arabi, H.; Boutorabi, M.A.; Seyedein, S.H.; Hasani Najafabadi, S.H. The effects of room temperature ECAP and subsequent aging on mechanical properties of 2024 Al alloy. *J. Alloys Compd.* **2014**, *585*, 753–759. [[CrossRef](#)]
35. Huda, Z.; Taib, N.I.; Zaharinie, T. Characterization of 2024-T3: An aerospace aluminum alloy. *Mater. Chem. Phys.* **2009**, *113*, 515–517. [[CrossRef](#)]
36. Bertocello, J.C.B.; Manhabosco, S.M.; Dick, L.F.P. Corrosion study of the friction stir lap joint of AA7050-T76511 on AA2024-T3 using the scanning vibrating electrode technique. *Corros. Sci.* **2015**, *94*, 359–367. [[CrossRef](#)]
37. Wang, P.; Gammer, C.; Brenne, F.; Niendorf, T.; Eckert, J.; Scudino, S. A heat treatable TiB<sub>2</sub>/Al-3.5Cu-1.5Mg-1Si composite fabricated by selective laser melting: Microstructure, heat treatment and mechanical properties. *Compos. B Eng.* **2018**, *147*, 162–168. [[CrossRef](#)]
38. Hekmat-Ardakan, A.; Liu, X.C.; Ajersch, F.; Chen, X.G. Wear behaviour of hypereutectic Al-Si-Cu-Mg casting alloys with variable Mg contents. *Wear* **2010**, *269*, 684–692. [[CrossRef](#)]

39. Liu, Z.; Chong, P.H.; Butt, A.N.; Skeldon, P.; Thompson, G.E. Corrosion mechanism of laser-melted AA 2014 and AA 2024 alloys. *Appl. Surf. Sci.* **2005**, *247*, 294–299. [[CrossRef](#)]
40. Ebrahimi, G.R.; Zarei-Hanzaki, A.; Haghshenas, M.; Arabshahi, H. The effect of heat treatment on hot deformation behaviour of Al 2024. *J. Mater. Process. Technol.* **2008**, *206*, 25–29. [[CrossRef](#)]
41. Rigney, D.A. The roles of hardness in the sliding behavior of materials. *Wear* **1994**, *175*, 63–69. [[CrossRef](#)]
42. Liu, R.; Li, D.Y. Modification of Archard's equation by taking account of elastic/pseudoelastic properties of materials. *Wear* **2001**, *251*, 956–964. [[CrossRef](#)]
43. Archard, J.F.; Hirst, W. The Wear of Metals under Unlubricated Conditions. *Proc. Math. Phys. Eng. Sci.* **1956**, *236*, 397–410.
44. Marceau, R.K.W.; Sha, G.; Lumley, R.N.; Ringer, S.P. Evolution of solute clustering in Al-Cu-Mg alloys during secondary ageing. *Acta Mater.* **2010**, *58*, 1795–1805. [[CrossRef](#)]
45. Starink, M.J.; Gao, N.; Davin, L.; Yan, J.; Cerezo, A. Room temperature precipitation in quenched Al-Cu-Mg alloys: A model for the reaction kinetics and yield strength development. *Philos. Mag.* **2005**, *85*, 1395–1417. [[CrossRef](#)]
46. Wang, F.; Liu, H.M.; Ma, Y.J.; Jin, Y.S. Effect of Si content on the dry sliding wear properties of spray-deposited Al-Si alloy. *Mater. Des.* **2004**, *25*, 163–166. [[CrossRef](#)]
47. Xiao, Q.; Liu, H.Q.; Yi, D.Q.; Yin, D.Y.; Chen, Y.Q.; Zhang, Y.; Wang, B. Effect of Cu content on precipitation and age-hardening behavior in Al-Mg-Si-xCu alloys. *J. Alloys Compd.* **2017**, *695*, 1005–1013. [[CrossRef](#)]